

Title: **Engineering Properties of Composite Mega-Columns with Separately Encased Hot Rolled Steel Profiles**

Authors: Chen Tao, Engineer, China Academy of Building Research
Fei Deng, PhD Candidate, Tsinghua University
Congzhen Xiao, Vice-Chief Engineer, China Academy of Building Research

Subject: Building Materials/Products

Keywords: Building Code
Composite
Concrete
Mega Column
Performance Based Design
Seismic
Steel
Structure

Publication Date: 2016

Original Publication: Cities to Megacities: Shaping Dense Vertical Urbanism

Paper Type: 1. Book chapter/Part chapter
2. Journal paper
3. **Conference proceeding**
4. Unpublished conference paper
5. Magazine article
6. Unpublished

© Council on Tall Buildings and Urban Habitat / Chen Tao; Fei Deng; Congzhen Xiao

Engineering Properties of Composite Mega-Columns with Separately Encased Hot Rolled Steel Profiles

分散型钢混凝土组合巨柱的力学性能研究



Congzhen Xiao | 肖从真
Vice-Chief Engineer | 副总工程师

China Academy of Building Research
中国建筑科学研究院

Beijing, China | 北京, 中国

Dr. Congzhen Xiao, who graduated from Tsinghua University, is now the Research Fellow, PhD Supervisor, and Vice-Chief Engineer of the China Academy of Building Research (CABR). He has been engaged in design, research, and consulting on super high-rise buildings for over twenty years.

肖从真博士毕业于清华大学土木工程系，现任中国建筑科学研究院副总工程师、研究员、博士生导师，在超高层建筑结构设计、研究及咨询领域有超过二十年的从业经验。



Chen Tao | 陈涛
Engineer | 工程师

China Academy of Building Research
中国建筑科学研究院

Beijing, China | 北京, 中国

Dr. Chen has been the engineer of China Academy of Building Research since 2009. He specializes in seismic design of tall buildings and experimental study on tall buildings and structural members.

陈涛博士自2009年起担任中国建筑科学研究院的工程师，专门从事高层建筑的抗震设计以及高层建筑和结构构件的试验研究。



Fei Deng | 邓飞
PhD Candidate | 博士研究生

Tsinghua University
清华大学

Beijing, China | 北京, 中国

Fei Deng acquired his bachelors in Civil Engineering from Tsinghua University in 2013, and is now a PhD candidate affiliated with Tsinghua University and the China Academy of Building Research.

邓飞2013年从清华大学土木工程系毕业，取得学士学位，现为清华大学及中国建筑科学研究院联合培养博士研究生。

This paper was also authored by the following people: Jean Claude Gerardy, Senior Project Sales Manager, ArcelorMittal; Don Davies, President, Magnusson Klemencic Associates; Elenora Lucchese, Research Assistant, CTBUH; Nicolette Popa, Head of Structural Long Products, ArcelorMittal; Dario Trabucco, Research Manager, CTBUH/IUAV; Oliver Vassart, General Manager of Long Carbon sector R&D, ArcelorMittal

本文作者还包括: ArcelorMittal 高级项目销售经理 Jean Claude Gerardy, Magnusson Klemencic Associates 总裁 Don Davies, CTBUH 助理研究员 Elenora Lucchese, ArcelorMittal 结构长材主任 Nicolette Popa, CTBUH / IUAV 研究部经理 Dario Trabucco, ArcelorMittal 长碳部门研发总经理 Oliver Vassart



Abstract | 摘要

This paper presents an experimental study on the behavior of composite mega-columns with separately encased steel profiles. Ten scaled composite columns were designed, including six 1/4-scaled test specimens and four 1/6-scaled test specimens tested under static and quasi-static loads, respectively. The controlling parameter in this research was the eccentricity ratio of the applied loads. Results indicate that within the 15 percent eccentricity ratio, (1) full composite action between concrete and the steel profiles can be realized, even though the steel profiles are not connected with one another; (2) the current AISC-LRFD, Eurocode4, and Chinese code JGJ 138 are able to predict the flexural capacity of this kind of column with sufficient accuracy and a reasonable margin of safety; and (3) the deformation capacities of the specimens meet the minimum requirement specified by the codes. Finally, a simplified design method is provided in this paper. This research is initiated and sponsored by ArcelorMittal.

Keywords: Composite Action, Composite Mega-Column, Seismic Performance, Separate Steel Profile, Simplified Design Method

本文通过试验研究了内嵌分散型钢的混凝土组合巨柱的力学性能，共包括6个缩尺比例为1:4的静力试件及4个缩尺比例为1:6的拟静力试件。试验中的控制参数为荷载偏心率。结果表明，在15%的偏心率以内：（1）尽管型钢没有连接为一个整体，型钢与混凝土之间也可以实现完全组合作用；（2）美国钢结构规范AISC-LRFD、欧洲规范4及中国《型钢混凝土组合结构技术规程》等规范可以较准确地预测各试件的轴心受压及压弯承载力，并具有一定的安全余度；（3）试件的变形能力满足中国规范的要求。最后，本文验证了简化设计方法对分散型钢组合柱的适用性。本研究由安赛乐·米塔尔公司发起并资助。

关键词：组合作用、组合巨柱、分散型钢、简化设计方法

Foreword

This experimental program is supported and sponsored by ArcelorMittal (AM). The structural engineering firm Magnusson Klemencic Associates (MKA) provides background studies on composite mega-column projects. The Council on Tall Buildings and Urban Habitat (CTBUH) is the coordinator of this program. The China Academy of Building Research (CABR) is responsible for conducting experiments and drafting research papers. The authors gratefully acknowledge the contributions from these organizations.

Introduction

As urbanization plays a major role in economic growth and industrial transformation, super high-rise buildings are becoming important solutions to the effective use of limited space in mega cities. The structural optimization of tall buildings is a meaningful topic, as it offers approaches in minimizing the dimensions of structural elements, thus reducing material

前言

本研究项目由安赛乐·米塔尔公司（AM）发起并资助。此外，结构咨询顾问MKA为本项目提供了组合巨柱的背景资料，世界高层都市建筑学会（CTBUH）参与了项目的协调工作，中国建筑科学研究院（CABR）主要负责试验并撰写研究报告。作者对上述组织在研究中所做出的贡献表示衷心感谢。

简介

城市化是经济增长和产业升级的重要引擎，在此过程中，超高层建筑成为缓解城市用地空间日趋紧张的重要解决方案。结构优化设计是超高层建筑研究领域的重要组成部分，旨在减小结构构件尺寸，从而减少材料用量、节约成本、促进低碳环保，其中一种优化方法便是采用钢-混凝土组合构件。

为进一步实现超高层结构的优化，本文提出了一种新型内嵌分散型钢的混凝土组合柱（图1）。与采用整体型钢的组合柱相

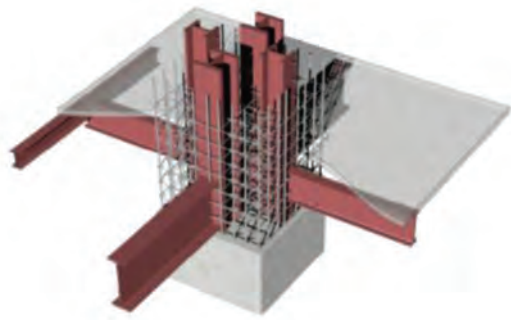


Figure 1. Mega-column with separate steel sections (Source: MKA)
图1. 分散型钢混凝土巨柱 (来源: MKA)

quantities costs and environmental impacts. Composite structural elements combining concrete and structural steel may accomplish this type of optimization.

A new type of composite column with separately embedded H-shape steel sections (Figure 1) is proposed for the further optimization of tall building designs. By using several separate steel sections instead of one single steel section embedded in the column, the welding works can be reduced considerably, thus saving construction time and costs. In addition, since the dimensions of the separately embedded H-shape steel members are relatively smaller than that of the single built-up jumbo steel used in traditional composite mega-column construction, the steel members can be directly fabricated in factory and transported to construction sites for erection. Consequently, quality control for the separate steel members in the factory will be easier than that of the structural steel welded in situ.

Behaviors of composite columns with single structural steel under static loads (Oh et al. 2006; Dundar et al. 2008) and simulated seismic loads (Shim et al. 2011; Naito et al. 2010; Yan et al. 2010) have already been well studied through physical tests and numerical analyses (Ellobody et al. 2011). Previous studies (Shen and Nie 1997; Nie and Cai 2003) revealed that the strength and rigidity of a composite beam is significantly affected by the degree of composite action between the concrete and the steel. Similarly, interface conditions between concrete and steel sections in composite columns may also affect the load transfer between these two parts, thus directly influencing the capacity and rigidity of composite columns. In regards to the performance of composite columns with separate steel sections, limited experiments have been conducted.

Different codes provide a variety of simplified methods to predict the capacity of composite columns with a single structural steel

embedded under combined compression and flexure, such as AISC-LRFD (2016), Eurocode4 (2004), and Chinese code JGJ 138 (2001). These codes are mainly based on the assumption that "plane sections remain plane." The composite action, however, has not been validated in composite columns with separate steel sections, so the applicability of the code provisions should be questioned for such kind of composite columns.

Ten test specimens were designed based on the 1.8-meter by 1.8-meter square composite mega-column of a real project to be constructed in China. Six 1/4-scaled test specimens and four 1/6-scaled test specimens were observed under static and quasi-static loads, respectively. Herein, preparations and results of the tests, together with discussions, are presented in the following two sections of this paper. Most of the discussions will be concentrated on the flexural capacity, deformation capacity, composition action, and seismic performance of the test specimens. Finally, a simplified design method is justified by comparing test results with code predictions.

Static Tests – Results and Discussions

Test Preparations

Six 1/4-scaled test specimens with identical dimensions and configurations are designed (Figure 2). The controlling parameter in static tests is the eccentricity ratio e/h , where e is the eccentricity of the vertical load, and h is the width of the composite cross-section. Specifically, specimen E00-1 and E00-2 are loaded with $e/h=0$; E10-1 and E10-2 with $e/h=10\%$; and E15-1 and E15-2 with $e/h=15\%$.

The test specimen has a 450-millimeter by 450-millimeter square cross-section with the structural steel ratio of $\rho_a=10.5\%$. Four 120-millimeter by 106-millimeter by 12-millimeter by 20-millimeter (height x width x web thickness x flange thickness) I-shaped,

分散型钢组合柱可以减少现场焊接量, 节约工期和成本。此外, 由于单个分散型钢的截面尺寸比中央整体式钢骨的截面尺寸更小, 使得这些分散的型钢可以在工厂制作完成后直接运至现场拼装, 从而实现更好的质量控制。

整体钢骨组合柱在静力荷载(Oh et al. 2006; Dundar et al. 2008)及低周往复荷载作用下(Naito et al. 2010; Yan et al. 2010; Shim et al. 2011)的力学性能已经得到了较充分的研究(Ellobody et al. 2011)。此外, 研究还表明, 钢-混凝土组合梁的承载力和刚度受钢-混凝土界面的连接程度影响较大(Shen and Nie 1997; Nie and Cai 2003)。类似的, 在组合柱中, 钢-混凝土的界面连接程度也会影响荷载在二者之间的分配, 从而影响组合柱的承载力和刚度。然而, 目前对分散型钢组合柱力学性能的试验研究还较少。

规范提供了多种简化方法用于计算整体钢骨组合柱的压弯承载力, 如美国钢结构规范AISC-LRFD (2016) (以下简称AISC-LRFD)、欧洲规范4 (以下简称EC4)、中国规范《型钢混凝土组合结构技术规程》(2001) (以下简称JGJ 138) 等。以上规范均基于平界面假定的原理计算组合构件的压弯承载力。然而, 在分散型钢组合柱中, 钢-混凝土之间能否发挥完全组合作用还未得到试验和理论上的证实, 因此上述规范是否适用于分散型钢组合柱仍有待商榷。

基于中国某工程实例(组合柱实际尺寸为1.8m x 1.8m), 本文共设计了10个试件, 其中包括6个1:4比例的静力试件和4个1:6比例的拟静力试件。文章分别对静力及拟静力试件的试验准备和试验结果进行了介绍, 并重点讨论了各试件的压弯承载力、变形能力、组合作用及抗震性能。文章最后通过将试验结果与规范计算值进行对比, 验证了简化设计方法在分散型钢组合柱中的适用性。

静力试验——结果及讨论

试验准备

本节共设计了6个尺寸及构造完全相同的试件(图2), 试验中的控制参数是荷载偏心率 e/h , 其中 e 为荷载偏心距, h 为试件截面宽度。试件E00-1及E00-2所受偏心率为0, E10-1及E10-2所受偏心率为10%, E15-1及E15-2所受偏心率为15%。

试件截面尺寸为450mm x 450mm, 含钢率10.5%。4个120mm x 106mm x 12mm x 20mm (高度x宽度x腹板厚度x翼缘厚度) 尺寸的热轧工字钢内嵌于混凝土中。除节点区外, 各型钢之间没有任何连接。型钢中心距截面中心127.5mm。

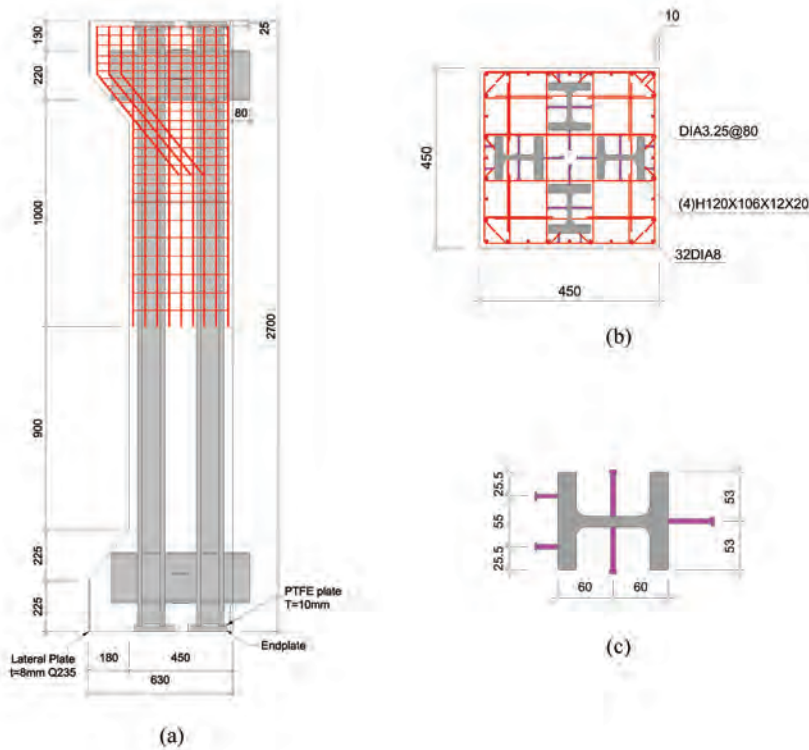


Figure 2. Dimensions and details of static specimens: (a) overall dimensions; (b) cross-section layout; (c) shear studs details (Source: CABR)

图2 静力试件尺寸及配筋: (a) 整体尺寸; (b) 截面构造; (c) 栓钉布置 (来源: 中国建筑科学研究院)

hot-rolled steel sections are embedded in the concrete without any connections with each other except at the beam-column joints. The distance between the center of the steel sections and the center of the cross-section is 127.5 millimeters. Shear studs are installed on the steel surfaces to enhance the composite action between the concrete and the steel with an interval of 144 millimeters. The diameter and length of the studs are six millimeters and 50 millimeters, respectively. Studs that are on the outside of the steel flanges are cut to 25 millimeters long to allow for sufficient concrete cover. The column length is 2,700 millimeters and there is a corbel at each column end for applying eccentric loads. Two I-shaped steel sections are installed at each end of the column to simulate the floor beams. The ends of the test specimens are confined by eight-millimeter-thick steel plates to ensure safety and to prevent premature failure during the test.

The test specimen is placed between two hinges (Figure 3). One hinge is placed on the ground and fixed by blocks to avoid any horizontal displacement. The other one is placed on the top of the test specimen, connected to a transition beam that serves as a connector between the hinge, horizontal actuators, and the vertical actuator. During the test, lateral displacement of the transition beam is strictly controlled by the horizontal actuators to ensure lateral displacement of the top end of the column is zero.

Sand layers are placed between the test specimen and the hinge, and PTFE (Polytetrafluoroethylene – a kind of soft and smooth plastic) plates are placed under endplates of the steel sections, so as to make sure that the concrete-steel interface slip can be developed near the test specimen ends to simulate real boundary conditions as precisely as possible. In real structures, relative slip may occur along the composite column at any point. If the sand layers and PTFE plates are not provided, the rigid surface of the hinge will force the test specimen end to stay in the same plane. Consequently, relative displacement between the concrete and the steel sections near the test specimen ends will be limited, which overestimates the composite action in the composite column. The material properties are listed in Figure 4.

Test Results and Discussions

The loading rate is slow enough to avoid dynamic effects. Loads are increased to peak value until the test specimen failed (axial loading capacity decreased for 15%). Since behaviors of several test specimens are similar herein, only test specimens E00-2 and E10-2 are introduced (Figure 5).

Test Specimen E00-2 is loaded without eccentricity; therefore, no lateral deformations are detected before the failure of the test specimen. Before the maximum capacity (P_u) is reached, only a few vertical cracks occur on the faces of the column due to very thin

为提高型钢与混凝土之间的组合作用, 型钢表面沿纵向每隔144mm布置一周直径为6mm、长度50mm的抗剪栓钉。其中, 由于型钢外翼缘外侧混凝土保护层厚度较薄, 该位置的栓钉长度缩短至25mm。试件总长度2700mm, 每端各有一个牛腿以施加偏心荷载, 并焊接两个互相正交的工字钢以模拟楼面梁。此外, 试件端部设置一圈8mm厚的钢板以保证安全, 同时可以防止端部过早破坏而影响试验结果。

试件安装在两个单向铰内(图3)。一个单向铰置于地面并限制住水平位移, 另一个单向铰位于试件顶部并与转换梁相连。转换梁进而与水平作动器和垂直作动器相连。试验过程中, 转换梁的水平位移由水平作动器严格限制, 从而保证试件的顶部不会发生水平侧移。

在试件端面与单向铰之间铺设一层砂垫层, 此外, 柱型钢的端板内部放置了聚四氟乙烯(PTFE)板。此举目的在于释放试件端部型钢与混凝土之间的相对滑移, 从而尽可能准确的模拟真实结构中的边界条件。真实结构中, 相对滑移可能在沿柱长度方向的任何位置发生。若不设置砂垫层和PTFE板, 则单向铰的刚性表面将迫使试件端面保持在一个平面内, 从而限制端部附近相对滑移的开展, 高估型钢与混凝土之间的组合作用。材料强度请见图4。

试验结果及讨论

加载过程中荷载缓慢增大以避免动力效应, 峰值点之后继续加载直至试件破坏(承载力下降15%)。由于试件的破坏过程相似, 本节仅以试件E00-2及E10-2为例介绍试件的破坏过程(图5)。

试件E00-2为轴心受力构件, 试件直至破坏之前都没有出现水平变形。当轴力达到最大荷载(P_u)时, 受混凝土保护层厚度较薄、栓钉的劈裂作用等因素影响, 试件表面正中出现了几道竖向裂缝。当最大荷载出现时, 试件上、下端角部混凝土由于端面压力的不均匀分布而发生开裂。受此影响, 试件两端发生旋转, 使得试件中部产生向左(有牛腿的一侧)的水平侧移, 造成试件中出现了二阶弯矩。最终, 试件由于中部混凝土的压溃而破坏。

与此相对, 试件E10-2表现出压弯破坏特征。当荷载上升至峰值荷载的50%时, 试件中部出现几道竖向裂缝, 原因与试件E00-2的竖向裂缝类似。随着荷载的增大, 试件中部的受压区竖向裂缝与受拉区水平裂缝同时开展。同时, 试件的水平侧移也在逐渐增加。最终, 试件中部受压区混凝土严重破坏, 试验停止。

尽管轴心受力试件和压弯试件最终的破坏形态相似, 但是二者的加载过程却明显不同(图6(a))。对于试件E00-1与E00-2, 轴向荷载在峰值点后出现了两次突降。第一次下降恰好出现在峰值承载力

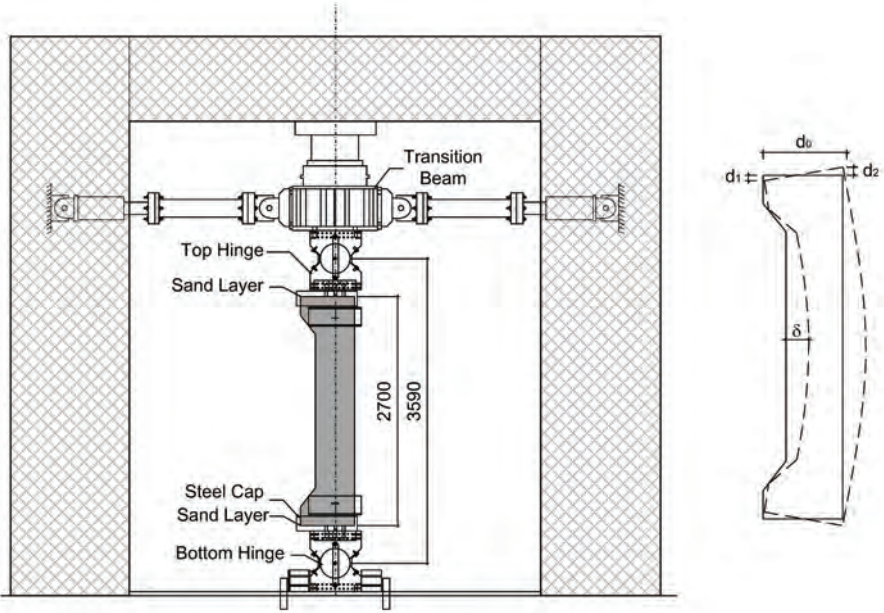


Figure 3. Set-up of static tests (Source: CABR)
图3. 静力试验加载装置 (来源: 中国建筑科学研究院)

Specimen ID	f_{ck} /Mpa	f_{yp} /Mpa		f_{ys} /Mpa	"Ntest/kN"	"Mtest/kNm"
		flange	web			
E00-1	47.9	408	423	438	17,082	143
E00-2	43.8	398	411		15,325	52
E10-1	47.6	423	435		14,360	803
E10-2	58.6	383	415		13,231	767
E15-1	52.4	377	404		12,041	1076
E15-2	53.8	389	405		12,759	1026
D10-1	56.2	458		459	7,427	308
D10-2	56.1				7,190	246
D15-1	53.7				6,153	306
D15-2	61.9				6,312	323

f_{ck} = concrete compressive strength
 f_{yp} = yield strength of structural steel
 f_{ys} = yield strength of longitudinal reinforcement

Figure 4. Tested material strengths and specimen capacities (Source: CABR)
图4. 实测材料及构件强度 (来源: 中国建筑科学研究院)

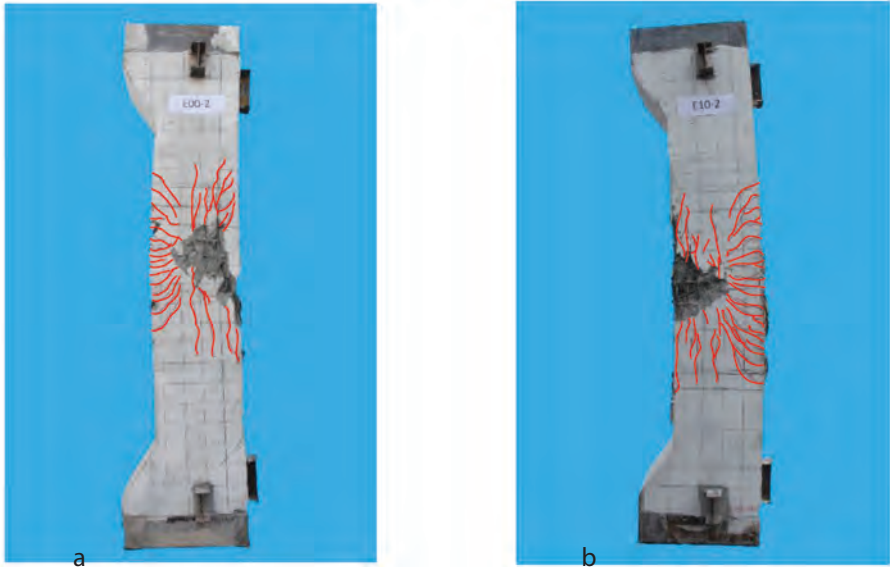


Figure 5. Crack distributions and failure modes of static specimens: (a) specimen E00-2; (b) specimen E10-2 (Source: CABR)
图5. 静力试件裂缝分布及破坏模式: (a) 试件E00-2; (b) 试件E10-2 (来源: 中国建筑科学研究院)

之后, 荷载迅速降至70% P_u 左右。接着, 竖向荷载由70% P_u 缓慢降至60% P_u , 同时竖向位移迅速增加。当荷载降至60% P_u 左右时, 试件中部混凝土突然压溃, 造成承载力第二次突降, 此时试件破坏。由于试件端部旋转产生的二阶效应, 试件的实测承载力实际上低于短柱轴心受压承载力 (详见下文)。另一方面, 偏心受压试件的承载力并没有出现突降。当到达峰值承载力后, 轴向荷载缓慢下降直至试件破坏。

试件中部截面的弯矩可以由下式计算:

$$M = P(e + \delta)$$

其中, P 为轴向荷载, e 为初始偏心距, δ 为试件在该截面处的水平侧移。截面曲率可以由应变分布得到。试验结果表明, 静力试件均表现出良好的曲率延性 (图6(b))。随着曲率的开展, 截面弯矩始终可以保持在较高水平, 主要原因在于: (1) 对于采用高强混凝土的构件, 型钢的屈服应变往往小于混凝土的峰值应变, 因此混凝土的应力下降后, 型钢的应力还可以进一步上升, 从而抵消混凝土导致的承载力下降, 使得截面整体的弯矩基本保持不变; (2) 随着混凝土损伤的积累, 截面弯矩逐渐由混凝土向型钢转移, 型钢与混凝土之间良好的组合作用保证了内力重分部得以实现。

拟静力试验——结果及讨论

试验准备

本节研究了4个1:6比例试件的拟静力加载试验 (图7)。试件截面尺寸为300mm x 300mm, 单个型钢截面尺寸为80mm x 70mm x 12mm x 12mm (高度x宽度x腹板厚度x翼缘厚度), 含钢率10.5%。型钢中心距截面中心85mm。栓钉的直径和长度分别为5mm和25mm。同静力试件类似, 型钢外翼缘的栓钉长度由于混凝土保护层厚度较薄而缩短至15mm。

在传统的低周往复加载试验中, 轴力一般通过竖向千斤顶施加, 而竖向千斤顶与反力架之间通过滑板相连。当试件受到水平荷载作用时, 竖向千斤顶可以通过滑轮随试件左右移动。然而, 滑轮表面的摩擦力往往很难准确测定。当竖向荷载较大时, 水平力的测量精度会受到影响。为解决摩擦力的问题, 本试验中将传统的悬臂柱上下对称复制, 得到一个十字形构件 (请见图6(a)), 一个构件实际上包含上、下两根柱。构件上、下端部通过单向铰与反力架相连, 从而形成一个静定体系以消除摩擦力的影响 (图8(a)(b))。水平荷载通过构件中部的水平作动器施加, 上、下两根柱所承受的剪力各自为水平荷载的一半。与静力试验同理, 拟静力试验中也布置了砂垫层及PTFE板。

concrete cover and the splitting effect caused by the shear studs. When the maximum capacity is reached, the corners of the column ends are cracked because of the unevenly distributed pressure on the test specimen surfaces. As a result, the ends rotate in the direction such that the mid-height cross section moves toward left (the corbel side), which leads to the occurrence of second order bending moment in the column. Finally, the column fails due to crush of the compressive concrete.

In comparison, test specimen E10-2 fails in combined compression and flexure pattern. Similarly, a few vertical cracks occur when the axial load reaches about 50% of the maximum load. As the load increases, vertical cracks and horizontal cracks continuously develop on the compressive side and tensile side of the column, respectively. Lateral deflection of the column is also developing. Finally, the test is stopped when the concrete on the compressive side is severely damaged.

Although the crack distributions at the failure level are similar for the test specimen subjected to pure axial load and the one subjected to eccentric axial load, the failure processes are quite different (Figure 6(a)). Axial loads of test specimen E00-1 and E00-2 show two sudden drops during the test. The axial load first drops to $70\%P_u$ very quickly, right after the maximum load is reached. Then, it gradually decreases from $70\%P_u$ to $60\%P_u$, while the vertical deflection is developing rapidly. When the axial load decreases to about $60\%P_u$, the second drop of axial load occurs, followed by the sudden crush of the concrete in the middle of the column. The rotation of the column end is registered after the first drop of the axial load, resulting

in lower tested capacities compared to the short-column axial resistances, which will be discussed in more detail later in this paper. On the other hand, no sudden drops in axial loads are detected for the test specimens subjected to eccentric axial loads. After the maximum loads are reached, axial loads of these four test specimens gradually decrease until failure.

The bending moment on the mid-height cross-section can be calculated using the following equation:

$$M = P(e + \delta)$$

P is the axial load; e is the initial eccentricity of the load; and δ is the lateral deflection at the middle point of the column. The curvature of the cross-section can be obtained based on the strain distribution. It is found that the deformation ductility of the static test specimens is excellent in terms of "moment versus curvature" (Figure 6(b)).

The higher flexural resistance of the composite column is able to sustain at a high level can be attributed to two reasons. First, the steel yields before the concrete reaches its peak compressive strength when high-strength concrete is used; therefore, the strengthening of steel may counteract the decrease in concrete's compressive strength to maintain the flexural resistance of the composite column. Second, the bending moment barely drops while the curvature is developing. With the cumulative damage of the concrete, the bending moment transfers from the concrete to steel sections due to stress redistribution. The desirable composite action between the concrete and the steel sections guarantees that the load transfer can be realized.

在真实结构中，柱中的轴力和剪力随地震作用强度的变化而同时变化。为此，本试验采用了一种两阶段加载方式来模拟真实地震作用（图8(c)）：

第一阶段仅施加竖向荷载。根据中国规范，轴压比定义为轴力设计值与短柱承载力设计值之间的比值，第一阶段轴力的大小 N_0 由下式确定：

$$ACR = \frac{\text{Design axial load}}{\text{Design short-column axial resistance}} = \frac{1.25N_0}{A_c f_c + A_s f_s + A_s f_s} = 0.7$$

其中， A_c 、 A_s 及 A_s 分别为混凝土、型钢和纵筋的面积， f_c 、 f_s 及 f_s 分别为上述三部分的强度设计值。带入相关数据可得，短柱承载力设计值为6184kN。式(2)中的0.7为JGJ 138规范允许的最大轴压比。可得，第一阶段的目标轴力 N_0 为3488kN，试验中实际取值3500kN。

在第二阶段中，轴力与水平力按预计偏心率所确定的路径同比例增加。每一级加载中，首先轴力增加500kN，然后保持轴力不变，水平力循环加载。试件D10-1与D10-2按10%偏心率路径加载，试件D15-1与D15-2按15%偏心率路径加载。材料实测强度请见图4。

试验结果及讨论

由于各试件的偏心率相差不大，故各试件的破坏模式相似——均为压弯破坏（图9）。当第一阶段加载完成后，试件中没有出现明显的变形和裂缝。在第二阶段加载中，混凝土表面的裂缝与损伤逐渐开展，最终试件均由于柱角部混凝土压溃而破坏。

当混凝土出现破坏或压溃后，暴露出的纵筋由于缺乏有效约束而发生屈曲失稳，但柱内型钢并没有表现出失稳的特性，主要是由于：（1）型钢的抗弯刚度本身较

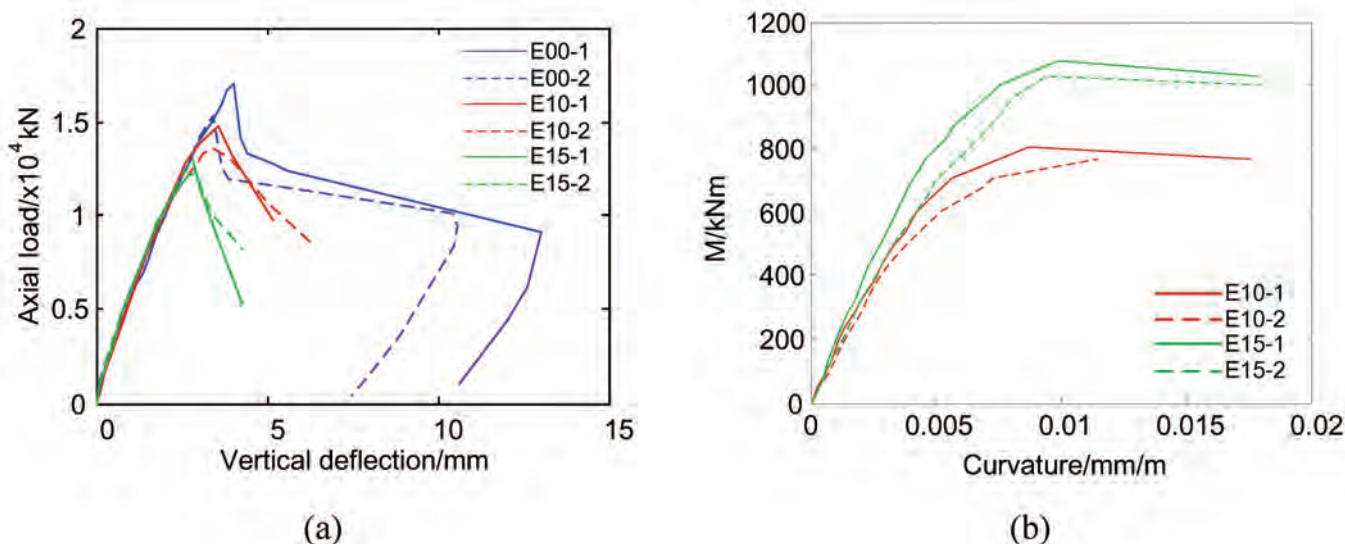


Figure 6. Loading curves of static specimens: (a) axial load vs. vertical deflection; (b) bending moment versus the curvature of the mid-height cross-section (Source: CABR)
图6 静力试验加载曲线：(a) 轴力 vs. 轴向变形；(b) 柱中弯矩 vs. 曲率（来源：中国建筑科学研究院）

Test Preparations

Four 1/6-scaled test specimens are tested under quasi-static loads (Figure 7). The cross-section dimension of the test specimens is 300 millimeters by 300 millimeters, and the size of the structural steel is 80 millimeters by 70 millimeters by 12 millimeters by 12 millimeters (height x width x web thickness x flange thickness) ($\rho_a=10.5\%$). The center of the steel sections is 85 millimeters away from the center of the cross-section. Shear studs used in these test specimens are five millimeters in diameter and 25 millimeters in length, respectively. Like static specimens, the outside shear studs are shortened to 15 millimeters because of the lack of concrete cover.

Traditional experiment set-ups suffer from friction problems when the axial load is extremely high in quasi-static tests. In these tests, the axial load is usually applied by the vertical actuator, which is allowed to move laterally via a roller mechanism. The friction on the surface of the roller, however, is very hard to calibrate, thus reducing the accuracy of measuring the lateral loads, especially when the axial load is very high. To solve this problem, the traditional T-shaped test specimen is duplicated upside down, resulting in a cross-shaped test specimen (Figure 8(a)). In this way, a single test specimen actually contains two columns: the upper and the lower. By employing pin connections at the ends of the test specimen, a statically determinate system can be created to eliminate the influence of the friction (Figure 8(a)(b)). Each end of the test specimen is encased in a hinge that is restricted by braces to avoid lateral displacement. The lateral loads are applied by two horizontal actuators in the middle of the test specimen. The shear force carried by each column is half the lateral load applied by the horizontal actuators, regardless of the friction. For the same purpose, sand layers and PTFE plates are also placed in quasi-static tests.

In real structures, the axial force and the shear force in a column vary simultaneously with the intensity of the earthquakes; therefore, a two-step loading protocol is used to simulate the seismic behavior of the composite column under earthquakes (Figure 8(c)).

During step one, only axial load is applied to the test specimen to represent the gravity load. The axial compression ratio (ACR) is defined as the design axial load divided by the design short-column axial resistance based on Chinese standard:

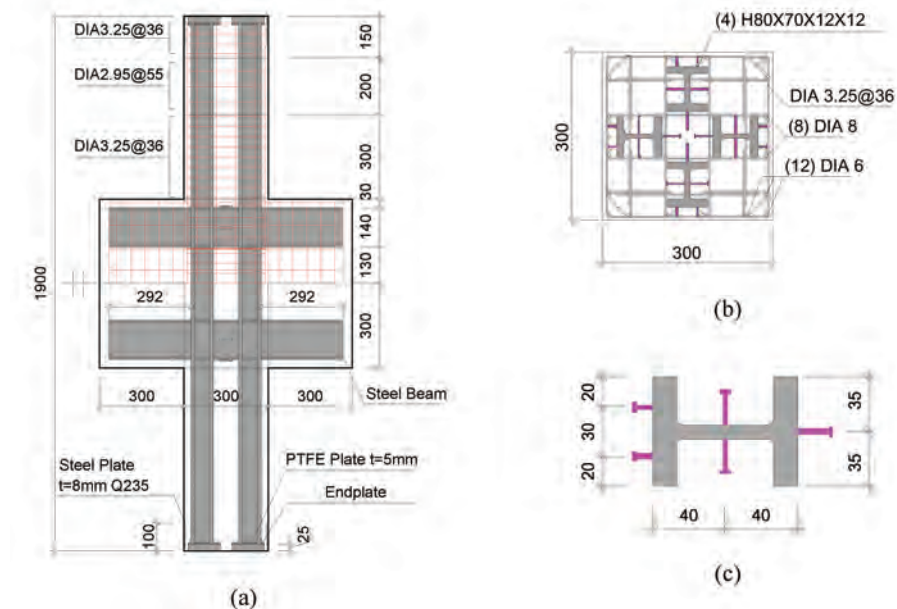


Figure 7. Dimensions and details of static specimens: (a) overall dimensions; (b) cross-section layout; (c) shear studs details (Source: CABR)

图7. 静力试件尺寸及配筋: (a) 整体尺寸; (b) 截面构造; (c) 栓钉布置 (来源: 中国建筑科学研究院)

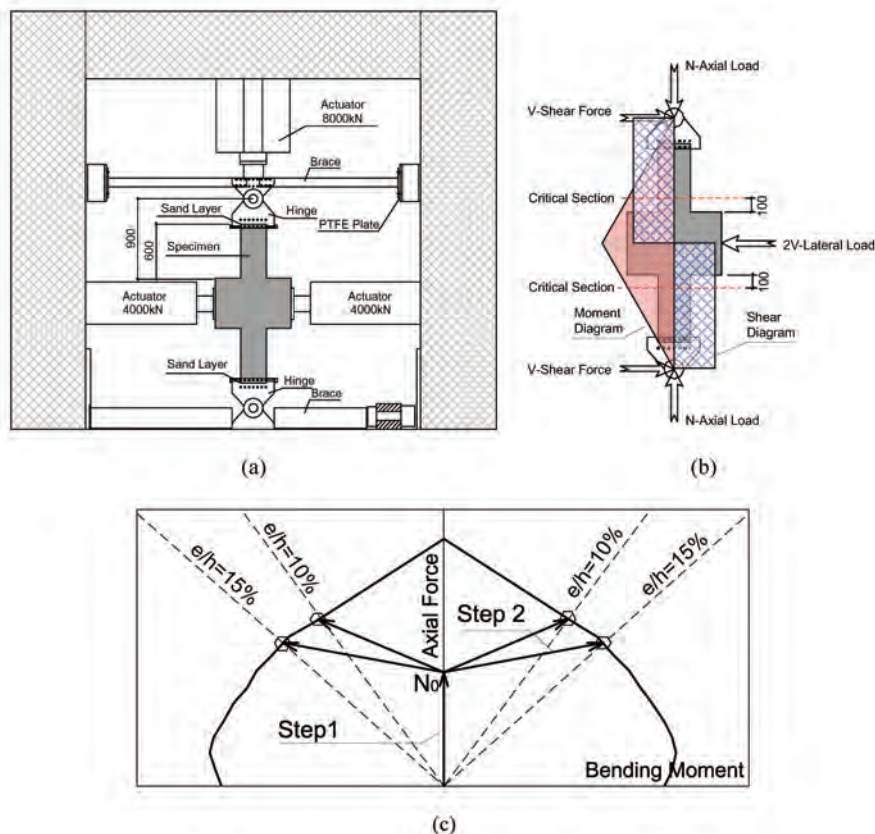


Figure 8. Set-up and loading protocols of quasi-static tests: (a) test set-up; (b) moment and shear diagram; (c) loading protocol (Source: CABR)

图8. 拟静力试验加载装置: (a) 加载装置; (b) 弯矩图及剪力图; (c) 加载制度 (来源: 中国建筑科学研究院)

$$ACR = \frac{\text{Design axial load}}{\text{Design short-column axial resistance}} = \frac{1.25N_0}{A_c f_c + A_s f_s + A_{st} f_s} = 0.7$$

A_c , A_{st} and A_s are the area of the concrete, steel sections, and longitudinal reinforcement, respectively; f_c , f_{st} and f_s are the design strengths of these three parts,

大, 不易发生失稳; (2) 核心区混凝土并没有发生明显破坏, 可以为型钢提供一定的侧向支撑, 有利于防止型钢发生屈曲失稳。

试验实测的剪力-顶点位移滞回曲线表明试件具有良好的耗能能力 (图10)。试验加载初期, 由于混凝土的开裂和型钢与混

respectively; N_o is the applied axial load at step one. By simple calculation, one can obtain that the design short-column axial resistance is 6184 kN. The value of 0.7 is the maximum allowable ACR specified by Chinese code JGJ 138 (2010); therefore, the target axial load N_o can be calculated as 3488 kN. In the test, N_o is set to 3500 kN.

During step two, the axial load and the lateral load increase proportionally to reach the target eccentricity ratio. Specifically, the axial load increases by 500 kN at the beginning of each cycle, and then the lateral load is applied cyclically, all while keeping the axial load constant. Test specimens D10-1 and D10-2 are loaded through the loading path with a 10% eccentricity ratio, while D15-1 and D15-2 are done with a 15% eccentricity ratio. The material properties are listed in Figure 4.

Test Results and Discussions

General behaviors of the quasi-static test specimens are quite alike because the eccentricity ratios do not differ much. Crack distributions and failure modes indicate that the test specimens fail in combined compression and flexure patterns (Figure 9). When the first step of the loading is completed, the test specimens do not show significant deformations and cracks. During the second step of the loading, cracks and concrete crush gradually develop, and the cumulative damage at the column corners leads to the failure of the test specimen.

When the outside concrete is damaged and crushed during the test, the longitudinal reinforcing bars begin to buckle due to lack of confinement. On the other hand, buckling failure is not detected for the steel sections. The primary reasons for this include: (1) the

stiffness of the steel sections is larger than that of the reinforcing bars; (2) the core concrete is not severely damaged, so that it is able to provide sufficient lateral restrictions to the steel sections to prevent buckling failures.

Hysteretic curves show the excellent energy consumption abilities of the quasi-static test specimens (Figure 10). The hysteretic curves show “pinch effect” in the beginning of the test because of the slip between the concrete and steel sections, as well as cracking of the concrete. The energy consumption is, therefore, limited when the lateral displacement is small. When the lateral displacement gets larger and the materials begin to yield, the energy consumption is mainly contributed by the plastic deformation of the materials. According to the hysteretic curves, energy consumption steadily increases, together with the increment of the lateral displacement.

The drift ratio is defined as the lateral displacement of the top of the column divided by the height of the column. The average drift ratio of test specimens D10-1 and D10-2 under ultimate load level (axial loading capacity decreased for 15%) is 1/79, and that of test specimens D15-1 and D15-2 is 1/67. Both of the deformation capacities meet the minimum requirements of 1/100 specified by Chinese code JGJ 3 (2010). Considering the high axial loads, the deformation capacities of the test specimens are beyond good. In addition, the average deformation capacity of test specimens D15-1 and D15-2 is 18% larger than that of test specimens D10-1 and D10-2, meaning larger eccentricity ratios could increase the deformation capacities of the columns.

混凝土之间的滑移等因素，滞回曲线表现出一定的“捏拢效应”。因此，当水平位移较小时，试件的耗能能力有限。当水平位移增大时，材料的塑性变形使得试件的耗能能力提升。试件的耗能能力随水平位移的增大而增大。

定义层间位移角为柱顶点水平位移与柱高的比值。在极限状态下（水平承载力下降15%），试件D10-1/D10-2与D15-1/D15-2的层间位移角均值分别为1/79和1/67，满足中国规范《高层建筑混凝土结构技术规程》（2010）中1/100的层间位移角限值要求。考虑到试验中的实际轴压比很高，试验所得的层间位移角足以验证各试件具有较好的变形能力。此外，15%偏心率的试件的层间位移角均值比10%偏心率的试件高18%，表明偏心率的增大有助于提高试件的变形能力。

简化设计方法

分散型钢组合柱中型钢的布置比较复杂，若按实际截面布置计算中和轴的位置，计算将非常复杂。因此，有学者提出利用塑性矩等效的方法将实际截面中的型钢和纵筋进行简化（图11）：

$$\left. \begin{aligned} h_1 &= h, b_1 = A_o / h_1 \\ h_2 &= b, b_2 = A_o / h_2 \end{aligned} \right\} \text{型钢}$$

$$\left. \begin{aligned} A_{s1} &= n_x A_s \\ h_{s1} &= (n_x - 1) s_x \\ b_{s1} &= A_{s1} / h_{s1} \\ A_{s2} &= (n_y - 2) A_s \\ h_{s2} &= (n_y - 3) s_y \\ b_{s2} &= A_{s2} / h_{s2} \end{aligned} \right\} \text{纵筋}$$

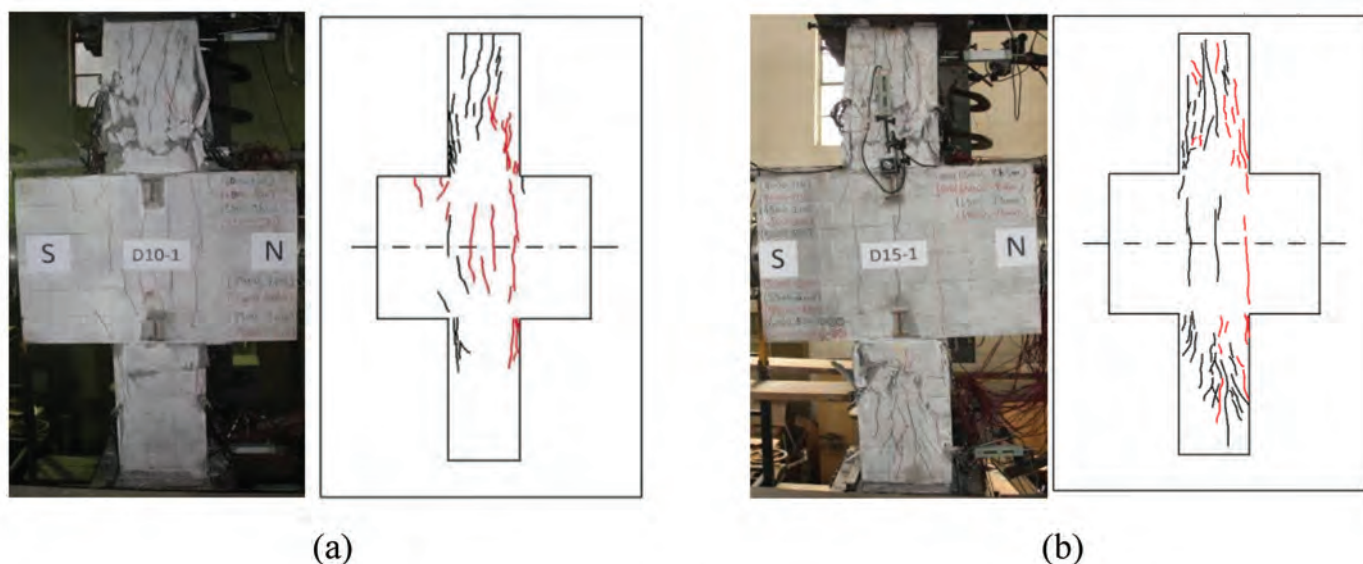


Figure 9. Crack distributions and failure modes of quasi-static specimens: (a) specimen D10-1; (b) specimen D15-1 (Source: CABR)
图9. 拟静力试件裂缝分布及破坏模式：(a) 试件D10-1；(b) 试件D15-1（来源：中国建筑科学研究院）

Simplified Design Methods

A simplified method is justified for the design of mega-columns with separate steel sections. Since the layout of structural steel is rather complicated in these kind of composite columns, it is impractical to locate the neutral axis of the actual composite cross-section. Researchers have therefore proposed simplified composite cross-sections based on the equivalent of plastic moment of inertia of the steel sections and longitudinal reinforcement (Figure 11):

$$\left. \begin{aligned} h_1 &= h, b_1 = A_a / h_1 \\ h_2 &= b, b_2 = A_a / h_2 \end{aligned} \right\} \text{for steel section}$$

$$\left. \begin{aligned} A_{s1} &= n_x A_s \\ h_{s1} &= (n_x - 1) s_x \\ b_{s1} &= A_{s1} / h_{s1} \\ A_{s2} &= (n_y - 2) A_s \\ h_{s2} &= (n_y - 3) s_y \\ b_{s2} &= A_{s2} / h_{s2} \end{aligned} \right\} \text{for longitudinal reinforcement}$$

n_x and n_y are the number of reinforcing bars along the width and height of the cross-

section, respectively. Previous studies (Plumier et al. 2014) have confirmed that simplification may guarantee sufficient accuracy when calculating the flexural capacity of the composite cross-section based on the plastic stress distribution method.

AISC (2016), Eurocode4 (2004), and Chinese code JGJ 138 (2001) provide a variety of ways to predict the flexural capacity of composite columns with a single encased structural steel section. According to these codes, the interaction curve can be calculated based on either the plastic stress distribution method or the plane section method, assuming that full composite action can be realized between the concrete and the structural steel. To justify the applicability of this design philosophy to composite columns with separate steel sections embedded, tested capacities of the specimens are compared with the code predictions assuming the full composite action.

The tested material strengths and test specimen capacities are listed in Figure 4. Note that although test specimens E00-1 and E00-2 are loaded with pure axial loads, bending moments are still detected on the mid-height

其中, n_x 和 n_y 分别表示沿截面宽度和高度方向上的纵筋数量。已有的研究表明,

采用简化后的截面, 根据截面的塑性应力分布计算其压弯承载力具有较高的精度 (Plumier et al. 2014)。

AISC-LRFD、EC4及JGJ 138规范提供了相应的简化方法计算整体钢骨组合柱的压弯承载力。根据上述规范, 假定型钢和混凝土之间可以实现完全组合作用, 则组合截面的压弯承载力可根据截面的塑性应力分布或平截面假定计算。假定分散型钢组合柱中亦可以实现完全组合作用, 利用现有规范的方法计算各试件压弯承载力并与试验结果进行对比, 可以验证简化方法在分散型钢组合柱中的适用性。

图4所示为各试件的实测材料强度及承载力。注意到, 尽管试件E00-1及E00-2为纯轴心受压构件, 但是试件中部截面由于二阶效应的影响仍然出现了弯矩。利用材料强度平均值分别计算静力试件及拟静力试件的相关线, 并与试验结果进行对比 (图12)。为使结果具有可比性, 计算截面的压弯承载力时, 暂不考虑稳定性及二阶效应的影响, 即, 相关线反映了组合截面的名义承载力。除轴心受力构件外, 其余各试件的规范预测承载力均偏于安全, 说明对于本试验中的构件, 截面的压弯承载力可以采用假定完全组合作用的简化计算方法。具体来讲, JGJ 138、EC4及AISC-LRFD的安全系数 (定义见图12) 平均值分别为1.03、1.17及1.40 (图13)。其中, AISC-LRFD给出的承载力计算值安全系数最高, 这是由于该规范采用双折线来近似代表实际的相关线, 使得相关线中部的压弯承载力被显著低估。与此相对, JGJ 138及EC4的计算结果比较接近。上述三个规范安全系数的标准差分别为0.08、0.10及0.20, 规范预测值与实际承载力之间的离散型较小。

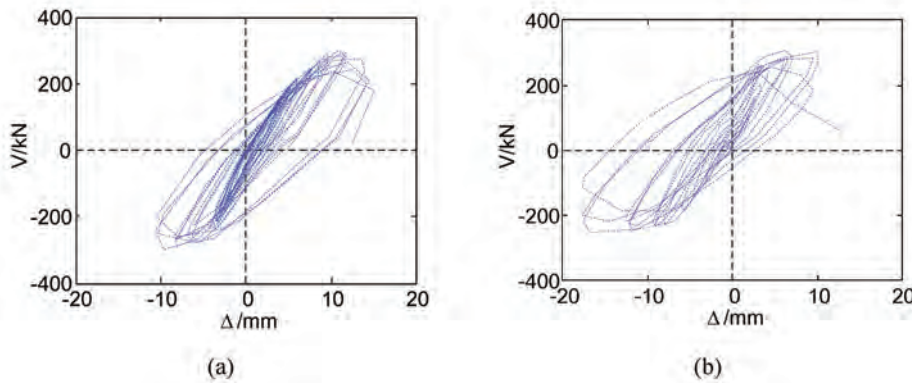


Figure 10. Hysteretic curves of quasi-static specimens: (a) specimen D10-1; (b) specimen D15-1 (Source: CABR)
图10. 拟静力试件滞回曲线: (a) 试件D10-1; (b) 试件D15-1 (来源: 中国建筑科学研究院)

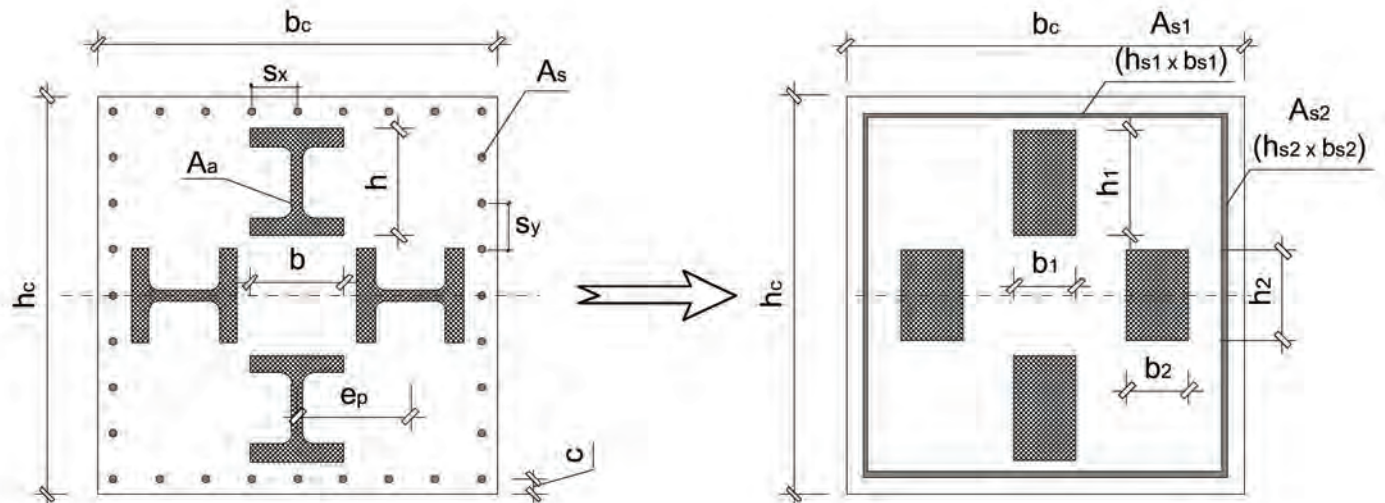


Figure 11. Simplification of the composite cross-section (Source: CABR)
图11. 组合截面简化方法 (来源: 中国建筑科学研究院)

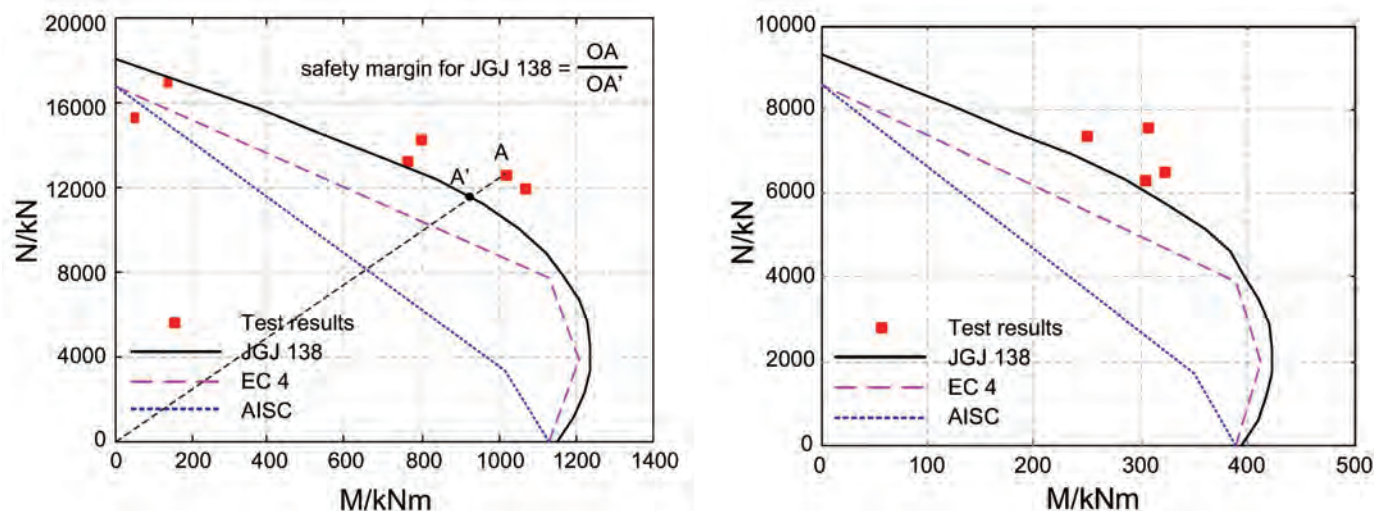


Figure 12. Test results and code predictions: (a) static tests; (b) quasi-static tests (Source: CABR)
图12. 试验结果及规范对比: (a)静力试验; (b)拟静力试验 (来源: 中国建筑科学研究院)

Specimen ID	JGJ 138	EC 4	AISC
E00-1	0.99	1.08	1.13
E00-2	0.87	0.94	0.96
E10-1	1.08	1.22	1.48
E10-2	1.01	1.15	1.39
E15-1	1.09	1.22	1.55
E15-2	1.10	1.25	1.55
D10-1	1.15	1.31	1.58
D10-2	0.95	1.21	1.44
D15-1	1.03	1.16	1.42
D15-2	1.07	1.21	1.49
AVE	1.03	1.17	1.40
STD	0.08	0.10	0.20

Figure 13. Safety margins of the code predictions (Source: CABR)
图13. 规范预测值的安全系数 (来源: 中国建筑科学研究院)

cross-sections of the test specimens due to lateral deflections. Test results and the code predictions are plotted in Figure 12, where the interaction curves are calculated based on the average tested material strengths. To make the results comparable, buckling effects and $P-\delta$ effects are not considered. Namely, the interaction curves represent the nominal strengths of the test specimens without considering any reduction factors. Results indicate that the tested capacities are all on the safe side except for test specimens subjected to pure axial loads, which suggests that assuming full composite action in the test specimen is feasible in terms of flexural capacity. Specifically, average safety margins (see definitions in Figure 12) of JGJ 138, Eurocode4, and AISC-LRFD are 1.03, 1.17, and 1.40, respectively (Figure 13). The AISC-LRFD is the most conservative one among these three codes, because it uses a bilinear line to represent the interaction

Specimen ID	N _{test} /kN	Short-Column Axial Resistance			Axial Resistance with Buckling Effects		
		JGJ 138	EC 4	AISC	JGJ 138	EC 4	AISC
E00-1	17,082	18,039	16,748	16,748	16,220	15,317	15,467
E00-2	15,325	17,089	15,909	15,909	15,415	14,600	14,722

Figure 14. Tested axial resistances and code predictions (Source: CABR)
图14. 实测轴心受压承载力及规范预测值 (来源: 中国建筑科学研究院)

curve, thus considerably underestimating the capacities in the middle part of the curves. On the other hand, JGJ 138 and Eurocode4 yield similar predictions. The standard deviations of the safety margins of the three codes are 0.08, 0.10, and 0.20, respectively, suggesting very little diversity among the code predictions.

As mentioned above, Figure 13 indicates that the code predictions can be unsafe for test specimens subjected to pure axial loads (E00-1 and E00-2), which is reasonable because these two test specimens obviously show slenderness effects during the tests. Therefore, in terms of pure axial resistances, a more appropriate way to justify the applicability of the code provisions is to compare the test results with code predictions to consider buckling effects. By doing so, the calculated axial resistances based on JGJ 138, Eurocode4, and AISC-LRFD with consideration to the buckling effects are relisted in Figure 14. It is clear that most of the code predictions are on the safe side when buckling effects are considered, except that JGJ 138 gives a larger code prediction on test specimen E00-2. This does not, however, necessarily mean that JGJ 138 is unsafe, because material partial factors and load factors have not yet been considered.

Note that test results used in this paper only confirm the effectiveness of current codes within the 15% eccentricity ratio. Since composite actions get weaker as the eccentricity ratio grows, the proposed

如前文所述, 图13所示结果表明对于轴心受压构件(试件E00-1及E00-2), 规范给出的截面轴心受压承载力与实测值相比可能偏于不安全。实际上, 由于试验中这两个试件均表现出了明显的长柱效应, 因此, 宜采用考虑稳定性后的轴心受压承载力与试验值进行比较。图14所列为考虑与不考虑稳定性影响时, JGJ 138、EC4及AISC-LRFD给出的轴心受压承载力计算值及试验结果。可以看到, 除JGJ 138对试件E00-2的承载力预测值大于试验值外, 其余各结果均偏于安全。由于本文还没有考虑材料分项系数及荷载分项系数等因素, 以上结果并不代表JGJ 138规范在实际设计中会造成不安全。

需要说明的是, 以上结论仅适用于偏心率不大于15%的分散型钢组合柱。由于型钢与混凝土之间的组合作用随偏心率的增大而降低, 除非经过试验或理论上的证实, 现有的简化方法并不适用于偏心率大于15%的分散型钢组合柱。

结论

本文提出了一种新型的分散型钢组合巨柱。由于单个型钢的截面尺寸减小, 其生产和运输问题均得以改善。此外, 焊接量的减小也简化了型钢的现场施工。为验证分散型钢组合柱的力学性能以及简化设计方法在计算压弯承载力时的适用性, 本文进行了两批试验, 所得结论如下:

simplified method cannot be applied to composite columns with separate steel sections when the eccentricity ratio is larger than 15%, unless the feasibility has been proved by either experiments or theoretical analyses.

Conclusions

A new type of composite mega-column embedded with multiple separate hot-rolled, steel H-shape sections is proposed in this paper. The production and transportation of the steel sections can be facilitated due to the reduced cross-section dimensions. In addition, easy erection of such mega-columns can be realized since the in situ welding works can be reduced considerably. Two series of experiments were conducted to validate the performance of this kind of composite column, and to justify the code provisions in determining axial and moment capacities. Conclusions of this paper are as follows:

- The test specimens fail in combined compression and flexure patterns.

Composite action between the concrete and steel can be realized under experimental conditions even though the steel sections are not connected to one another.

- Seismic performances of the test specimens are excellent in terms of curvature ductility, deformation capacities, and energy consumptions. Drift ratios of the test specimens exceed the minimum requirement by 26%~49%, specified by Chinese codes. Hysteretic curves of the test specimens are round and stable, and no sudden drops of the lateral loads are detected.
- Within the 15% eccentricity ratio, AISC-LRFD, Eurocode4, and JGJ 138, based on the plastic stress distribution method, are capable of providing accurate predictions on the flexural capacities of this kind of composite columns with rational safety margins. By considering buckling effects, code predictions on the pure axial resistances can also be safe and accurate.

- 所有试件均表现为压弯破坏模式，在试验条件下，型钢与混凝土之间的组合作用可以得到充分的发挥。
- 试验试件具有良好的曲率延性、变形能力及耗能能力。极限状态下的变形能力（层间位移角）超出中国规范所要求的最低限制26%~49%。试件的滞回曲线较饱满，水平承载力在峰值点后缓慢下降。
- 在15%的偏心率以内，AISC-LRFD、EC4及JGJ 138规范中基于截面塑性应力分布或平截面假定的简化计算方法可以较准确的预测分散型钢组合柱的压弯承载力，并具有一定的安全余度。考虑稳定性影响后，上述规范亦适用于轴心受压承载力的预测，计算结果同样较为准确且偏于安全。

References:

- American Institute of Steel Construction. (2016). **Load and Resistance Factor Design Specifications for Structural Steel Buildings** (AISC-LRFD). Chicago.
- Dundar, C., Tokgoz, S., Tanrikulu, A. K. and Baran, T. (2008). **Behaviour of Reinforced and Concrete-Encased Composite Columns Subjected to Biaxial Bending and Axial Load**. Building and environment, 43(6), 1109-1120.
- Ellobody, E., Young, B. and Lam, D. (2011). **Eccentrically Loaded Concrete Encased Steel Composite Columns**. Thin-Walled Structures, 49(1), 53-65.
- Eurocode 4 (2004). **Design of Composite Steel and Concrete Structures-Part 1.1: General-General Rules and Rules for Buildings**. EN 1994-1-1, Brussels.
- JGJ 138 (2001). **Technical Specification for Steel Reinforced Concrete Composite Structures**. Beijing.
- Naito, H., Akiyama, M. and Suzuki, M. (2010). **Ductility Evaluation of Concrete-Encased Steel Bridge Piers Subjected to Lateral Cyclic Loading**. Journal of Bridge Engineering, 16(1), 72-81.
- Nie, J.G., and Cai, C.S. (2003). **Steel-Concrete Composite Beams Considering Shear Slip Effects**. Journal of Structural Engineering, 129(4), 495-506.
- Oh, M.H., Ju, Y.K., Kim, M.H. and Kim, S.D. (2006). **Structural Performance of Steel-Concrete Composite Column Subjected to Axial and Flexural Loading**. Journal of Asian Architecture and Building Engineering, 5(1), 153-160.
- Plumier A., Bogdan T. and Degée H. (2014). **Design of Column with Several Encased Steel Profiles for Combined Compression and Bending**. Unpublished.
- Shen J.M. and Nie J.G. (1997). **Slip Effect on Strength of Composite Steel Concrete Beams**. China Civil Engineering Journal, 1, 005.
- Shim, C.S., Chung, Y.S. and Yoon, J.Y. (2011). **Cyclic Behavior of Prefabricated Circular Composite Columns with Low Steel Ratio**. Engineering Structures, 33(9), 2525-2534.
- Yan F., Xiao C.Z. and Xu P.F. (2010). **Experimental Study on the Irregular Shaped Steel Reinforced Concrete Columns of the China World Trade Center Phase III in Beijing**. China Civil Engineering Journal, 43(8), 11-20.